RESEARCH ARTICLE

In vivo quantitative MRI: T_1 and T_2 measurements of the human brain at 0.064 T

Kalina V. Jordanova[1] · Michele N. Martin[1] · Stephen E. Ogier[1,2] · Megan E. Poorman[3] · Kathryn E. Keenan[1]

Abstract

Objective To measure healthy brain T_1 and T_2 relaxation times at 0.064 T.

Materials and methods T_1 and T_2 relaxation times were measured in vivo for 10 healthy volunteers using a 0.064 T magnetic resonance imaging (MRI) system and for 10 test samples on both the MRI and a separate 0.064 T nuclear magnetic resonance (NMR) system. In vivo T_1 and T_2 values are reported for white matter (WM), gray matter (GM), and cerebrospinal fluid (CSF) for automatic segmentation regions and manual regions of interest (ROIs).

Results T_1 sample measurements on the MRI system were within 10% of the NMR measurement for 9 samples, and one sample was within 11%. Eight T_2 sample MRI measurements were within 25% of the NMR measurement, and the two longest T_2 samples had more than 25% variation. Automatic segmentations generally resulted in larger T_1 and T_2 estimates than manual ROIs.

Discussion T_1 and T_2 times for brain tissue were measured at 0.064 T. Test samples demonstrated accuracy in WM and GM ranges of values but underestimated long T_2 in the CSF range. This work contributes to measuring quantitative MRI properties of the human body at a range of field strengths.

Keyword Magnetic resonance imaging

Introduction

The field of quantitative magnetic resonance imaging (qMRI) is concerned with extracting characteristic biomarkers from a magnetic resonance (MR) image that have physical units attached to them [1, 2]. Methods for qMRI have been developed for measuring length and volume, relaxation properties (T_1, T_2, T_2*), fluid flow, diffusion, phase, fat fraction, proton density, etc. To achieve clinical utility of these methods, accurate knowledge of quantitative values for healthy and diseased tissue is critical [3, 4].

There has been renewed interest in MRI at field strengths ≤ 0.55 T for point-of-care diagnostics due to lower cost, greater portability, quieter operation, improved implant safety, reduced susceptibility artifacts, increased accessibility, and reduced limitations on the specific absorption rate while imaging compared to conventional MR systems (1.5 T and 3 T) [5]. Several scanners that operate at field strengths ≤ 0.55 T are in development [6–15]. Many companies have products available or under development at lower field strengths, including at 0.064 T (Swoop, Hyperfine, Guilford CT, USA), 0.066 T (Promaxo Inc., Oakland CA, USA), 0.345 T (MRIdian Linac, ViewRay, Mountain View CA, USA), 0.4 T (Magnifico Open, Esaote, Genoa, Italy), 0.5 T (Synaptive Medical Inc., Toronto, Canada), 0.55 T (MAGNETOM Free.Max, Siemens Healthineers, Erlangan, Germany), and at undisclosed field strengths (neuro42, San Francisco CA, USA). A natural extension of lower field MRI is to adopt qMRI methods, for which accurate knowledge of quantitative tissue properties at the relevant field strength is crucial. In the past, many in vivo quantitative measurements at field strengths ≤ 0.55 T have suffered from hardware limitations, causing trade-offs between feasibility and accuracy [16, 17]. Although there has been increased investigation into healthy brain relaxation parameters at lower

✉ Kalina V. Jordanova
kalina.jordanova@nist.gov

1 Physical Measurement Laboratory, National Institute of Standards and Technology, NIST, Boulder, CO, USA

2 Department of Physics, University of Colorado Boulder, Boulder, CO, USA

3 Hyperfine, Inc., Guilford, CT, USA

field strengths [18], additional measurements are necessary for each specific field strength and hardware, and for ensuring reproducibility of qMRI measurements.

We measure T_1 and T_2 relaxation parameters in the brain using a commercially-available 0.064 T MRI system. We design and test the in vivo measurement protocols by measuring test sample relaxation times on the 0.064 T MRI system and comparing them to 0.064 T NMR T_1 and T_2 measurements. T_1 and T_2 tissue values for white matter (WM), gray matter (GM), and cerebrospinal fluid (CSF) are reported.

Materials and methods

Measurement systems

Measurements were conducted on a 0.064 T Hyperfine Swoop MRI scanner (hardware 1.8, software rc8.3.1, Guilford CT, USA) using an 8-channel receive, 1-channel transmit head coil. The study was conducted in accordance with IRB guidelines, and all subjects provided informed consent. Additionally, the National Institute of Standards and Technology Research Protections Office reviewed and approved the research protocol, and the study was performed in accordance with the ethical standards as laid down in the 1964 Declaration of Helsinki and its later amendments.

Relaxation time measurements for a set of test samples were made on a Bruker variable field electromagnet nuclear magnetic resonance (NMR) system set to a field strength of 0.064 T, using a Redstone spectrometer and TNMR software (Tecmag, Houston, TX, USA). A custom RF copper solenoid coil was used, which was designed to allow perfluorocarbon coolant (TMC Industries, Inc., Waconia, MN, USA PN: FC-40) to flow around the sample for temperature control.

Test sample synthesis protocols

Test samples were prepared by dissolving stock solutions of metal compounds into deionized water. Specifically, the compounds used included $CuSO_4 \cdot 5H_2O$ (Millipore-Sigma, St. Louis, MO, USA; Part number (PN): 209198), $GdCl_3 \cdot 6H_2O$ (Millipore-Sigma, St. Louis, MO, USA; PN: 203289), edetic acid (EDTA) (Millipore-Sigma, St. Louis, MO, USA; PN: 324503), and $NiCl_2 \cdot 6H_2O$ (Millipore-Sigma, St. Louis, MO, USA; PN: N6136). $GdCl_3$-EDTA was made by stirring a $GdCl_3$ and EDTA (at twice the mmol/L value of $GdCl_3$) solution on a 98 °C hotplate for 30 min. Dry agarose (Millipore-Sigma, St. Louis, MO, USA; PN: A6013) was weighed and added to the paramagnetic salt solution, followed by heat cycles: (1) 30 s interval microwave cycle until boiling; (2) 10 min hotplate cycle to ensure well-hydrated

agarose. Deionized water was added to the mixture to make up for mass lost to evaporation. The mixture was poured into 50 ml or 30 ml sample tubes, pre-washed with isopropyl alcohol.

The selected test samples were: 0.1 mmol/L $CuSO_4$, 2 mmol/L $CuSO_4$, 0.75 mmol/L $CuSO_4$ in 0.25% agarose mass concentration (%), 1 mmol/L $CuSO_4$ in 1% agarose mass concentration (%), 0.025 mmol/L $GdCl_3$-EDTA, 0.1 mmol/L $GdCl_3$-EDTA in 1.5% agarose mass concentration (%), 4 mmol/L $NiCl_2$ in 1.2% agarose mass concentration (%), 0.1% agarose mass concentration (%), 0.5% agarose mass concentration (%), and deionized water. These samples were chosen for their expected similarity in T_1 and T_2 to WM, GM, or CSF at 0.064 T.

Quantitative imaging protocols

Optimization of T_1 mapping protocol via simulation

T_1 maps were acquired using an inversion recovery (IR) sequence, chosen for its robustness in T_1 measurements compared to other T_1 mapping methods [19].

The T_1 measurement protocol was optimized to acquire accurate values for WM, GM, and CSF in a feasible scan time for in vivo use. The repetition time (TR) and inversion times (TIs) were chosen by the following optimization process: (1) simulating the expected IR signal in the presence of noise; (2) solving for T_1 using the noisy simulations and IR signal equation; and (3) choosing the protocol that minimized the error in estimated T_1.

Specifically, MR signals were simulated for T_1 values in the range of 0.1 s to 4 s using the IR signal equation [20]:

$$S_i = S_0 \left| 1 - (1 + d)e^{-\frac{TI_i}{T_1}} + e^{-\frac{TR}{T_1}} \right| + n_i \qquad (1)$$

with S_i as the simulated signal for the ith TI, scale factor for imperfect inversion d (set to 0.95), and nominal signal intensity for a voxel S_0. A total of 25 simulations of Eq. 1 with additive Rician noise (n_i) [21] were used to estimate T_1, from which a mean T_1 estimate was calculated. The nominal signal magnitude S_0 was varied such that the signal-to-noise ratio (SNR) of the simulated signals ranged from 5 to 95. An SNR of 95 corresponds to the SNR observed in IR scans of the test samples. The ranges of TI_i and TR that were tested were selected such that the total scan time for the T_1 mapping protocol would be less than one hour.

T_1 was estimated from the simulated signals S_i for each [TI_i, TR] combination, and the optimal protocol was chosen such that it minimized simulated T_1 error for a range of SNR values, especially for the target tissue T_1 values (as given in [18]). While there was not one protocol with optimal performance for all SNR values, the optimal protocol was selected

for particularly good performance for SNR between 50 and 95, and reasonably good performance for SNR down to 25. Below an SNR of 25, all protocol simulations degraded substantially in their T_1 estimation capability.

T$_1$ mapping protocol

T_1 Maps were acquired using a research version of the Hyperfine T_1-weighted IR 3D fast spin echo (FSE) sequence.

The optimized protocol resulted in a TR of 2.4 s and TIs of 0.05 s, 0.15 s, 0.35 s, 0.5 s, 0.95 s, 1.995 s. Images were acquired with a 1.6 mm^2 in-plane resolution and 5 mm slice thickness, with a field of view of 22 cm $\times$ 18 cm $\times$ 18 cm. Each IR scan time was 9 min and 46 s, leading to a total IR session time of 58 min and 48 s, not including pre-scan calibration and localizer sequences. The total scan session time was typically around 61 min.

T$_2$ mapping protocol

To acquire T_2 maps, a research version of a Hyperfine T_2-weighted 3D FSE sequence with 10 echo times (*TE*s) was used. The protocol had a TR of 3 s and TEs of 0.037 s, 0.111 s, 0.185 s, 0.259 s, 0.333 s, 0.407 s, 0.480 s, 0.554 s, 0.628 s, 0.702 s, and was acquired on a spiral-out k-space trajectory with two dummy echoes. Images were acquired with a 1.5 mm^2 in-plane resolution and 5 mm slice thickness, with a field of view of 22 cm $\times$ 18 cm $\times$ 18 cm. The T_2 mapping sequence scan time was 17 min and 8 s, not including pre-scan calibration and localizer sequences. A typical total scan session time was around 20 min.

MRI measurements

In vivo measurements

In vivo T_1 and T_2 measurements were acquired using the protocols described above from 10 healthy volunteers (5 male, 5 female, ranging from 20 to 56 years old). Due to the extended scan time for each imaging protocol and to minimize strain on volunteers, quantitative measurements were acquired over two sessions for each volunteer. The average inter-session time was 9.3 days, with 8 volunteers having an inter-session time of less than or equal to 8 days, and two volunteers having longer inter-session times of 29 days and 42 days.

NMR measurements

T_1 and T_2 measurements were acquired for the test samples using the in vivo protocols described above on the 0.064 T MRI system, using a custom Hyperfine-provided phantom that held the 50 ml sample tubes. Additionally, T_1

measurements were acquired on the 0.064 T MRI system using a reference protocol with 29 *TI*s that is prohibitively long for in vivo scanning (*TI*s of 0.1 s, 0.15 s, 0.2 s, 0.25 s, 0.3 s, 0.35 s, 0.4 s, 0.45 s, 0.5 s, 0.55 s, 0.6 s, 0.7 s, 0.8 s, 0.9 s, 1.0 s, 1.1 s, 1.2 s, 1.3 s, 1.4 s, 1.5 s, 1.6 s, 1.7 s, 1.8 s, 1.9 s, 2.0 s, 2.1 s, 2.2 s, 2.3 s, 2.4 s; *TR* of 2.8 s; 1.6 mm^2 in-plane resolution; 5 mm slice thickness; and total imaging time of approximately 5.5 h).

For the T_1 NMR measurements, an IR sequence was used with 20 exponentially increasing *TI*s in steps of [0.001*x to x], with x being sample-dependent and ranging from 2.5 s to 15 s, selected such that the largest inversion time was longer than 5 times the expected T_1. For the T_2 NMR measurement, a Carr-Purcell-Meiboom-Gill (CPMG) sequence was used with 20 linearly increasing *TE*s in steps of [0.05*x to x] with x being sample-dependent and ranging from 0.08 s to 3.76 s, selected such that the longest echo time was 2.5 times to 3 times the expected T_2. For both T_1 and T_2, a final delay time of 5 times the expected T_1 was used. The samples for the NMR measurements were kept at 21.3 °C, the approximate temperature of the laboratory housing the 0.064 T MRI system.

Quantitative parameter analysis

Quantitative parameter map reconstruction

For all quantitative parameters, we assumed one quantitative value per voxel, and partial volume effects were not taken into account.

T_1 was calculated for each voxel using least squares minimization (lmfit, Python) for the IR model mentioned earlier [20]:

$$S_i = S_0 \left| 1 - (1 + d)e^{-\frac{TI_i}{T_1}} + e^{-\frac{TR}{T_1}} \right| \qquad (2)$$

where T_1 is the target value for the fit. For long T_1 and in the presence of noise, the in vivo protocol is ill-conditioned and results in very large estimated error in the T_1 measurements, on the order of the measurement itself. Thus, in vivo T_1 measurements were excluded when the standard error of the fit exceeded the measurement itself. A total of 14 voxels out of 80,389 total voxels were excluded.

The T_2 map was calculated for the Hyperfine protocol using non-linear least squares optimization (SciPy optimize_fit curve_fit, Python) for the model:

$$S_i = S_0 e^{-\frac{TE}{T_2}} \qquad (3)$$

where T_2 is the target value for the fit. A monoexponential decay was assumed and used to fit Eq. 3 directly to the image-space data.

Test sample region of interest selection

For T_1 and T_2 maps of the test samples acquired with the 0.064 T MRI system, regions of interest (ROIs) were selected using an automated protocol that searched for circles of the expected 50 ml tube size in each image slice. Once each tube was identified for each slice, the ROI of each tube was limited to a central circular region of half the tube's image radius. T_1 was fit using data from all voxels located in each ROI simultaneously, which resulted in one T_1 per ROI and per slice. T_2 values came directly from the Hyperfine software, and the mean of the T_2 value for all voxels in each ROI was calculated to give one T_2 value per ROI per slice. Finally, the six central slices of the phantom were selected due to their clean ROI tube segmentations compared to slices near the ends of the tubes, which had ROI segmentations that sometimes included the ends of the tube. The final reported T_1 and T_2 values represent the mean and standard deviation of each tube's ROI over these central six slices.

For 0.064 T NMR measurements, three repeated measurements were acquired for both T_1 and T_2, and the reported mean and standard deviation for each sample were calculated over the three replicate measurements. T_2 was calculated using Eq. 3, whereas because the NMR measurements used $TR > 5*T_1$, T_1 was calculated using a simplified form of Eq. 2, namely:

$$S_i = S_0 \left| 1 - (1 + d)e^{-\frac{TI_i}{T_1}} \right| \tag{4}$$

In vivo image segmentation

For in vivo images, T_1 and T_2 were calculated on a per-voxel basis using Eqs. 2, 3 for a slice chosen to be approximately centered on the ventricles, such that the anterior horn is well visualized. The skull was stripped away from each in vivo map using a thresholding-open-close image transformation series of operations. For T_1, the raw IR images were used in 8 of 10 volunteers to aid in the skull stripping.

A segmentation algorithm inspired by O'Reilly & Webb [18] was implemented to distinguish WM, GM, and CSF. A mixture of Gaussians was used with Python Scikit-learn Gaussian Mixture (GMM) to model the acquired T_1 or T_2 measurements, and voxels were binned into one of the tissue compartments based on the T_1 or T_2 value. To attempt to account for potential partial volume mixture between CSF and GM, a "partial" volume bin was included in the segmentation algorithm for tissue segmentation. Additionally, as in previous work [18], T_2 was indistinguishable for WM and GM using the auto-segmentation mixture of Gaussians method, and it was thus segmented as one tissue.

Manual selection of ROIs for WM, GM, and CSF were created via visual inspection of the raw images, the relaxation parameter maps, and the automatic segmentations. Small regions of 2 voxels × 2 voxels were selected by locating visually dissimilar areas to attempt to identify WM from GM in the right frontal lobe. For CSF, a region was selected wherever the ventricles showed the highest relaxation values. Manual CSF ROIs were selected from the right side for 5 volunteers, from the left side for 5 volunteers. The automatic segmentation results were used as a reference such that manually selected ROIs only included voxels from one automatically segmented region.

Statistical analysis

Relaxation time measurements for test samples using the NMR system versus the MRI system were compared by plotting the 95% confidence interval using the mean and standard deviation of each test sample, on each system. All MRI protocol measurements were normalized to the respective NMR measurement for each sample and relaxation parameter. Measurements that had overlapping 95% confidence intervals were said to be similar.

Bland–Altman plots were used to compare in vivo measurements from the manually selected ROIs to the measurements using the automatic segmentations. T_1 and T_2 were normalized to the average measurement value before calculating paired averages and differences for the Bland–Altman plots.

Results

Simulation results of estimated versus actual T_1 were used to select an optimized T_1 protocol (Fig. 1a) and resulted in a mean error in T_1 estimation of 2.03%. For comparison, simulation results from two non-optimal test protocols had mean errors in T_1 estimation of 39.0% and 187% (Fig. 1b, c).

To better understand measurement uncertainty, test samples were used to compare T_1 and T_2 measurements from the MRI system to measurements made using the 0.064 T NMR (Fig. 2). The Supplementary Information Table S.1 lists the test sample mean and standard deviation for the measurements shown in Fig. 2. T_1 measurements using the optimized in vivo MRI protocol had mean difference from the NMR measurements of 5.82% (Fig. 2a) and was acquired in one hour. By comparison, a reference MRI protocol that used 15 TIs and was acquired in 5.5 h had mean difference from the NMR measurements of 3.28% (Fig. 2b). All T_1 measurements were within 10% of the NMR measurement, except for 0.025 mmol/L GdCl$_3$-EDTA, which has an 11% difference between the NMR measurement and in vivo MRI protocol.
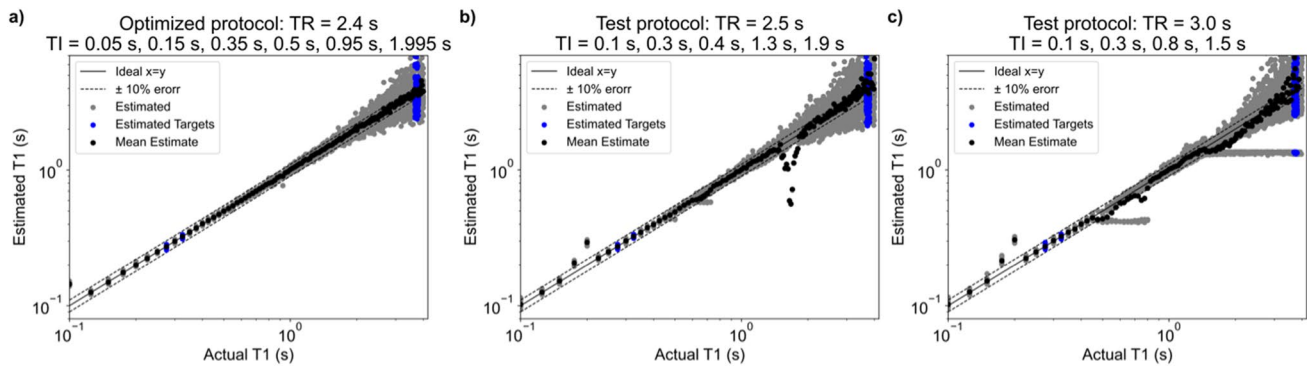
Fig. 1 **a** Simulation results of estimated versus actual T_1 for the selected in vivo T_1 mapping protocol. Six *TI* s were selected with a repetition time of 2.4 s, resulting in a total scan time of 60 min. Gray dots indicate each T_1 estimate of 25 simulations with added noise; black indicates the mean over the 25 noisy estimates; blue indicates estimated T_1 for the target expected T_1 values of WM, GM and CSF at 0.064 T. **b** Similar to plot (**a**), simulation results of an example suboptimal T_1 mapping protocol that would greatly overestimate T_1 of around 0.2 s, and greatly underestimate T_1 around 2 s. **c** Similar test protocol to (**b**), but with a longer *TR* and one fewer *TI* s, resulting in worse T_1 estimation overall. SNR = 95 was used to simulate (**a–c**)

For the test samples, the T_2 measurements using the in vivo MRI protocol had a mean difference from the NMR measurements of 20.1% (Fig. 2c). Eight samples have T_2 MRI measurements that lie within 25% of the NMR measurement, with 3 samples having MRI measurements within 10% of the NMR measurements. Specifically, for $T_2 \leq 1.27$ s, MRI and NMR measurements are within 25% of each other. For $T_2 \geq 1.27$ s, the in vivo MRI T_2 mapping protocol greatly underestimates T_2 compared to the NMR measurements.

The test sample measurement uncertainty was further quantified using confidence intervals of the in vivo MRI protocol measurements compared to confidence intervals of the NMR system measurements (Fig. 2d). T_1 measurements using the NMR system and measurements using the reference MRI protocol had overlapping 95% confidence intervals for all samples except 0.025 mmol/L GdCl$_3$-EDTA and 2 mmol/L CuSO$_4$. Comparing the NMR system to the in vivo MRI protocol, 0.025 mmol/L GdCl$_3$-EDTA, 2 mmol/L CuSO$_4$, and 0.75 mmol/L CuSO$_4$ in 0.25% agarose mass concentration (%) had non-overlapping 95% confidence intervals. Seven of 10 T_2 MRI measurements were not within the 95% confidence interval range of the NMR measurements.

The efficacy of the skull stripping algorithm is explored in Supplementary Information Fig. S.1. Example in vivo IR images from the optimized T_1 protocol are shown for one volunteer, and the full T_1 map for the same volunteer and the skull stripped version are shown for comparison, where the raw IR image for *TI* of 0.05 s was used to aid in skull stripping for this volunteer. An example T_2 map and skull stripping result for a different volunteer are also shown. Based on qualitative observation, the skull stripping algorithm sufficiently removed the skull without affecting brain soft tissue.

T_1 and T_2 measurements normalized to the average measured value for each volunteer and each segmentation type are plotted in Fig. 3. A summary of T_1 and T_2 measurement results for each volunteer and each segmented ROI is shown in the Supplementary Information Table S.2. Averages over all participants for each segmentation type and tissue are given. For T_1, the manual ROI averages are 0.254 s $\pm$ 0.0179 s for WM, 0.377 s $\pm$ 0.0351 s for GM, 2.073 s $\pm$ 1.2007 s for CSF. For T_2, the manual ROI averages are 0.081 s $\pm$ 0.0024 s for WM, 0.105 s $\pm$ 0.0241 s for GM, 1.172 s $\pm$ 0.3234 s for CSF. For T_1, the automatically segmented averages are 0.294 s $\pm$ 0.0179 s for WM, 0.46 s $\pm$ 0.1258 s for GM, 1.854 s $\pm$ 1.2097 s for CSF. For T_2, the automatically segmented averages are 0.097 s $\pm$ 0.0016 s for combined WM and GM, 0.553 s $\pm$ 0.1422 s for CSF. Two volunteers had manually segmented T_1 ROIs with lower CSF measurements than the automatic segmentations. In one volunteer, the highest CSF T_1 measurement was near the frontal lobe rather than in the ventricles where the manual ROIs were located. In the other, the measured T_1 in the ventricles was the highest of any volunteer, and selecting a square region for the manual ROI could not capture all of the highest T_1 values.

Variations were observed across volunteers in head size, ventricle size, the range of measured T_1 and T_2, and automatic segmentation regions (Figs. 4 and 5). A volunteer with typical outcomes is shown (Figs. 4a and 5a). A volunteer with the smallest head size by voxel count (subject 3 of Supplementary Information Table S.2) has lower CSF measurements compared to other volunteers (Figs. 4b and 5b). A volunteer with qualitatively larger ventricles shows higher CSF measurements compared to other volunteers (Figs. 4c and 5c).
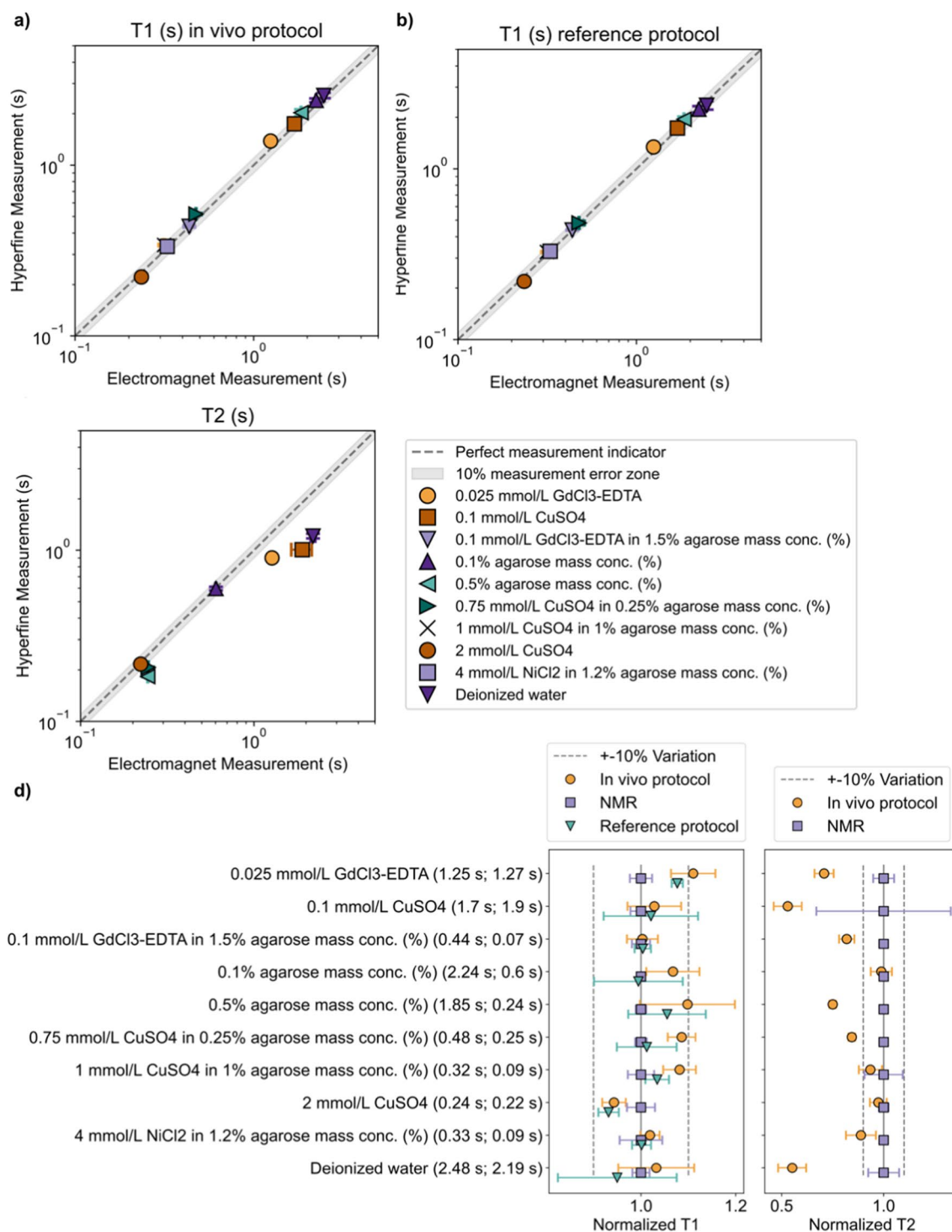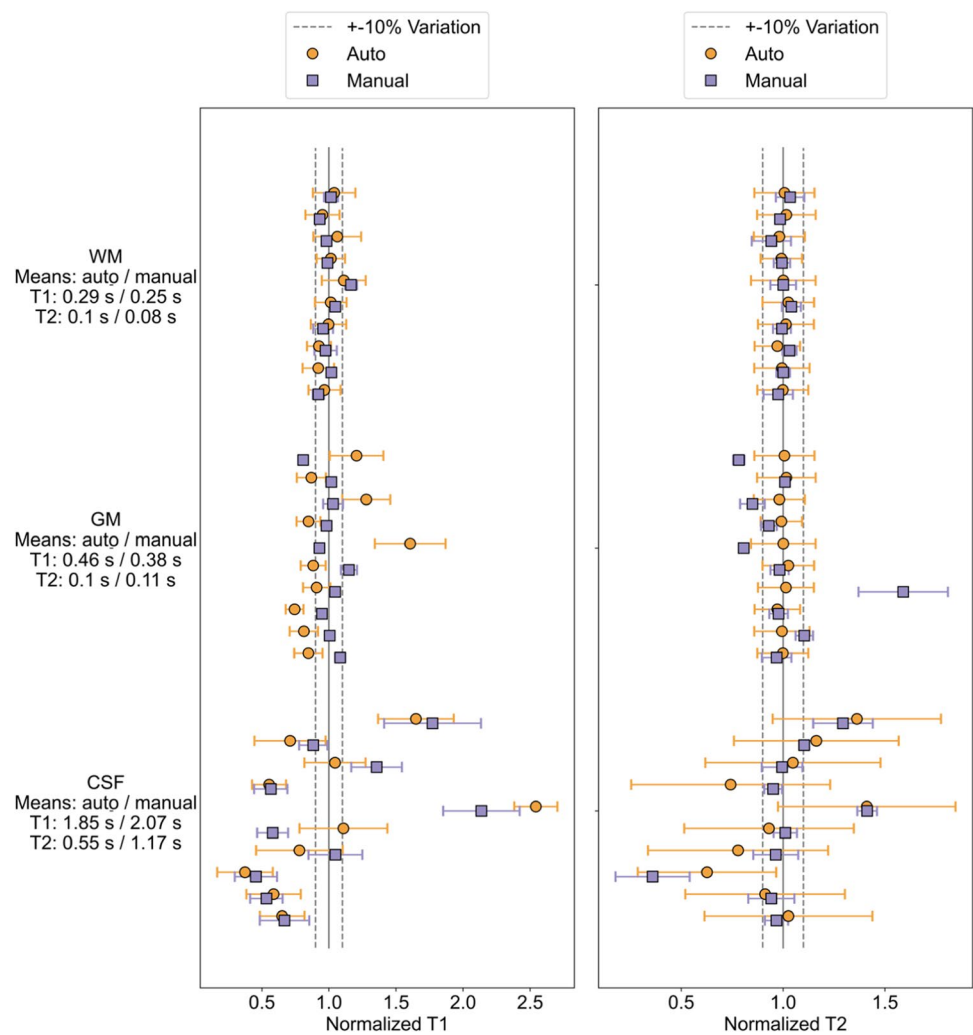
Fig. 2 **a–c** Sample validation results for the Hyperfine scan protocols compared to measurements made on an NMR electromagnet set to 0.064 T. **a** T_1 test sample results using the in vivo MRI protocol (1 h scan time) compared to the NMR measurements. **b** T_1 test sample results using a reference MRI T_1 protocol (5.5 h scan time) compared to NMR measurements. **c** T_2 test sample in vivo MRI protocol results compared to NMR measurements. **d** Comparisons for test sample T_1 (left) and T_2 (right) measurements using the NMR measurements as a reference versus the MRI in vivo and reference protocols. Measured NMR (T_1, T_2) values are shown next to each material label. Averages and 95% confidence intervals are plotted for each sample and measurement type

Fig. 3 Each volunteer's T_1 (left) and T_2 (right) mean measurements, with standard deviation shown as error bars. Mean T_1 and T_2 values are shown below tissue labels for auto/manual segmentations


Discussion

In vivo relaxation properties at 0.064 T were measured for 10 adult volunteers. The protocols used to measure relaxation were optimized when possible, and their accuracy was examined using test samples measured on a 0.064 T NMR system.

Differences in in vivo tissue T_1 and T_2 measurements between manually selected ROIs and automatic segmentations were explored using Bland–Altman plots (Fig. 6). T_2 for GM has mean differences of less than 10% between the two ROI creation methods. Other tissues all have less than 20% mean difference between the methods, except for CSF T_2, which has 72% mean difference between the measurements. Finally, the variance in the differences between the ROI creation methods are smaller for WM and GM than for CSF.

Measurement protocols

T_1 And T_2 measurement protocols suitable for in vivo use were developed and validated. The T_1 in vivo protocol was designed to minimize expected error in measured T_1, while keeping the total scan time to be one hour. Simulations of protocols that used fewer TI s resulted in overall worse T_1 estimation than when using additional TI s. However, the scan time limitation required the use of a shorter TR when the number of TI s was increased. Overall, this resulted in a T_1 protocol that can have an ill-conditioned fit for high values of T_1 when the noise in the image is large. Thus, a tradeoff was made between scan time and expected accuracy in high T_1 measurements, resulting in a higher coefficient of variation for the CSF T_1 measurements compared to WM and GM. A limitation to this study is that the T_1 fitting protocol did not account for Rician noise in the IR magnitude images, which can improve fitting outcomes [22, 23].

Test samples were used to validate both of the T_1 and T_2 in vivo MRI protocols compared to an NMR measurement,
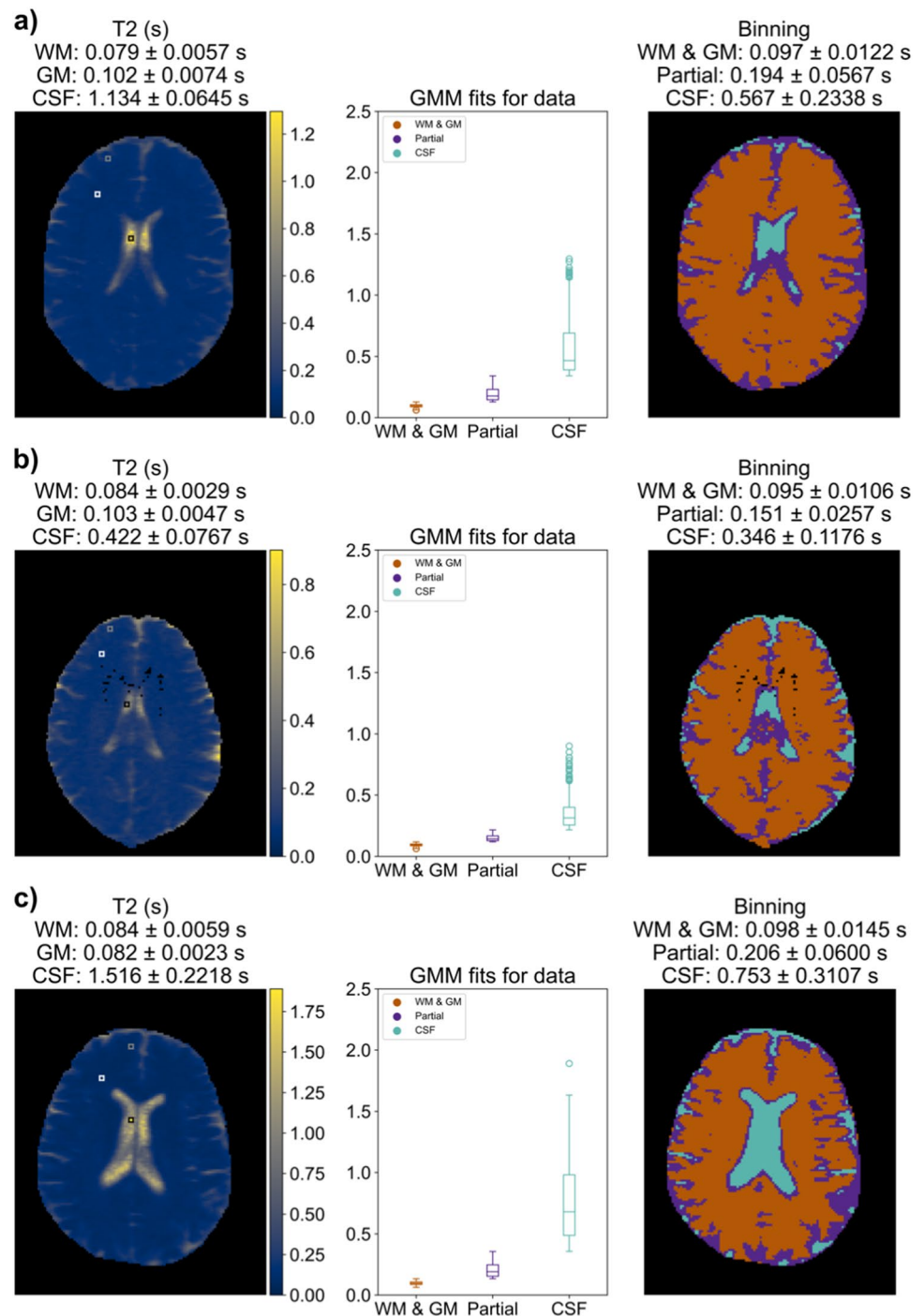
Fig. 4 Each row shows one of 3 example T_1 in vivo measurements: (left) T_1 maps with visual indications of manually selected ROIs for WM (white), GM (gray), and CSF (black); (middle) T_1 values by auto-segmented bin; (right) visual map of the auto-segmented bins. Mean and standard deviation of T_1 are indicated for each manual or auto-segmented ROI. **a** A subject exhibiting a typical T_1 map for this study. **b** A subject with small head size showing lower CSF values, likely due to partial volume effects from smaller ventricles. **c** An example subject with large ventricles and a higher CSF measurement
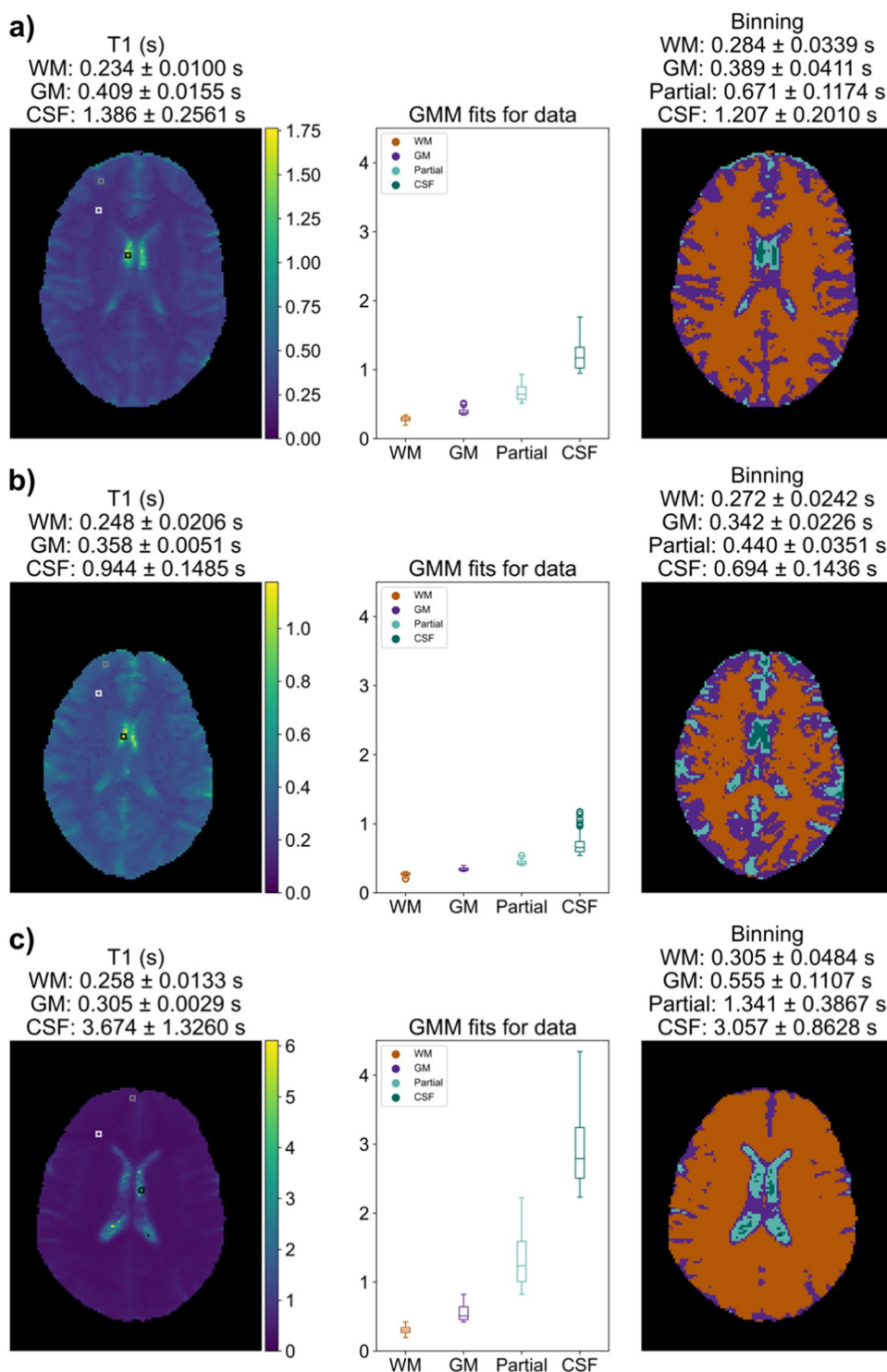
as well as a reference MRI protocol for T_1. Test samples demonstrated accuracy in the WM and GM range of values but underestimated large T_2 in the CSF range. A limitation of this study is the underestimation of T_2 using the MRI in vivo protocol for CSF, and care should be taken when interpreting CSF T_2 results. There are a few confounds that

could influence the accuracy of the long T_2 measurements. Spurious signal pathways due to system imperfections are more likely to compound in long T_2 species, making them more susceptible to errors. Furthermore, the fast spin echo acquisition that was modified to build the T_2 mapping sequence was designed to generate clean clinically

Fig. 5 Each row shows one of 3 example T_2 in vivo measurements for the same volunteers of Fig. 4: (left) T_2 maps with visual indications of manually selected ROIS for WM (white), GM (gray), and CSF (black); (middle) T_2 values by auto-segmented bin; (right) visual map of the auto-segmented bins. Mean and standard deviation of T_2 are indicated for each manual or auto-segmented ROI. **a** A subject exhibiting a typical T_2 map for this study. **b** A subject with small head size showing lower CSF values, likely due to partial volume effects from smaller ventricles. **c** An example subject with large ventricles and a higher CSF measurement

In vivo measurement results

Measured in vivo relaxation values can be compared to relaxation values reported in literature for 0.05 T [18], namely for T_1: 0.275 s for WM, 0.327 s for GM, 3.695 s for CSF; and for T_2: 0.102 s for WM, 0.102 s for GM, 1.584 s for CSF. The automatic segmentation results for WM and GM of this study are closer to previous literature results than the
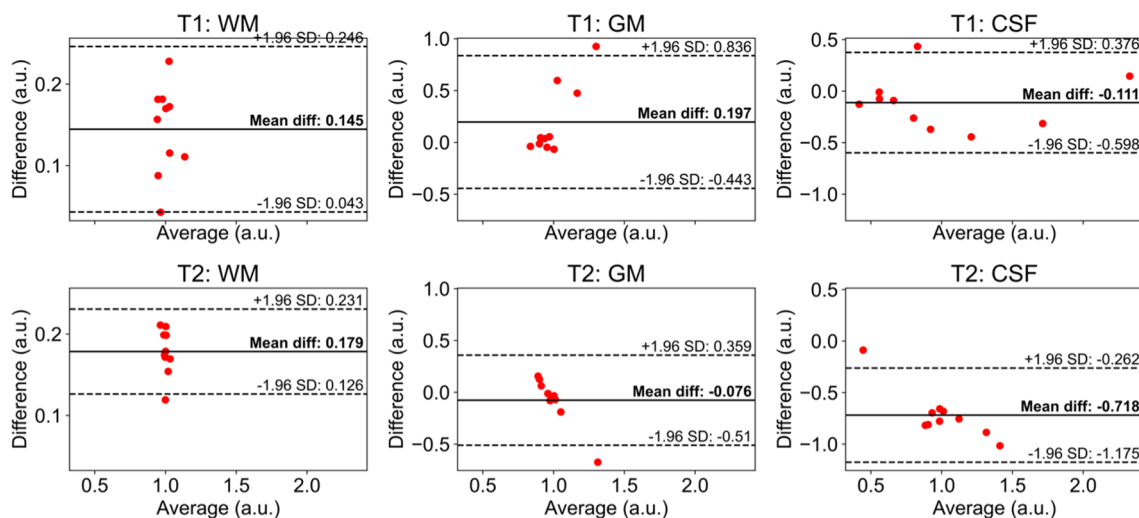
useful images in harsh electromagnetic environments. It is not clear how the proprietary steps necessary to ensure good clinical image quality would affect the expected signal decay. Finally, magnitude images were used for the T_2 fit which could bring a Rician noise influence into the data. The T_2 model could be modified to account for Rician noise, or to include a constant term in the fitting. These modifications were not explored in this study.

Fig. 6 Bland–Altman plots for in vivo measurements using the manual ROIs compared to the automatic segmentations. The differences are calculated as the automatic segmentation measurement minus the manual ROI measurement. Mean differences are marked as the black line and ± 1.96 standard deviations from the mean difference are indicated with dashed lines

manual ROIs, with T_1 of 0.294 s for WM and 0.46 s for GM, and T_2 of 0.097 s for WM and GM.

As mentioned previously, the T_2 measurements for CSF are likely underestimations of the true values due to limitations of the measurement protocol. However, partial volume effects from the 5 mm slice thickness may also cause underestimations in both the T_1 and T_2 measurements. Challenges in accurately measuring CSF are known: earlier studies underestimated T_1 relaxation in CSF due to repetition time settings that were too short [16, 17]. To remove partial volume effects, more recent work at 0.05 T developed a separate protocol specifically targeted to isolate signal when measuring relaxation in CSF [18]. Future work is needed to accurately measure relaxation in CSF at 0.064 T.

In vivo skull stripping and tissue selection methods

A skull stripping protocol was developed and demonstrated to work effectively at removing background noise and the skull from in vivo quantitative maps. To calculate average T_1 and T_2 times for different tissues, two tissue selection methods were compared. One was an automatic segmentation method and the other used manually selected ROIs. Similar to previous work at a similar field strength [18], we found that the relatively small difference between WM and GM relaxation parameters made it difficult to segment and analyze the two tissues independently, especially using our automatic segmentation method. An improvement to the study would be to acquire anatomical images during scanning; however, for this study it was not possible to acquire anatomical images during the T_1 protocol due to scan time limitations.

To compare average relaxation times using the two tissue selection methods, Bland–Altman plots were used. A large mean difference was observed between the tissue selection methods for CSF T_2, likely because the highest region of measured T_2 was targeted when creating manual ROIs. While the manually selected ROIs could introduce selection bias, the automatic segmentation method could also be biased because the binning method uses the underlying T_1 and T_2 measurements, thus, tissue designation is determined from the relaxation parameter itself in the automatic segmentation algorithm. Ideally a segmentation method would designate tissue independently from the relaxation measurement of a voxel.

Conclusion

Tissue relaxation measurements for T_1 and T_2 at 0.064 T have been measured and presented for 10 healthy volunteers. Two ROI selection methods were used for determining mean T_1 and T_2 for the volunteers. Test samples were measured on a 0.064 T NMR and a 0.064 T MRI system, and the measurements were compared. This work will contribute to the growing body of research targeted at measuring and disseminating qMRI properties of the human body for a wide range of field strengths.

Author contributions Jordanova contributed to the study conception and design, acquisition of data, analysis and interpretation of data, drafting of manuscript, and critical revision. Martin contributed to the acquisition of data, analysis and interpretation, and critical revision. Ogier contributed to the acquisition of data, analysis and interpretation, and critical revision. Poorman contributed to analysis and interpretation of data, and critical revision. Keenan contributed to study conception and design, analysis and interpretation of data, drafting of manuscript, and critical revision.

Data availability The authors confirm that the data supporting the findings of this study are available within the article and its supplementary materials.

Declarations

Conflict of interest The authors declare that they have no conflict of interest. Certain commercial equipment, instruments, or materials are identified in this paper in order to specify the experimental procedure adequately. Such identification is not intended to imply recommendation or endorsement by NIST, nor is it intended to imply that the materials or equipment identified are necessarily the best available for the purpose.

Ethical approval The study was conducted in accordance with IRB guidelines. Additionally, the National Institute of Standards and Technology Research Protections Office reviewed and approved the research protocol, and the study was performed in accordance with the ethical standards as laid down in the 1964 Declaration of Helsinki and its later amendments.

Informed consent All subjects provided informed consent.

References

1. Rosenkrantz AB, Mendiratta-Lala M, Bartholmai BJ, Ganeshan D, Abramson RG, Burton KR, Yu J-PJ, Scalzetti EM, Yankeelov TE, Subramaniam RM, Lenchik L (2015) Clinical utility of quantitative imaging. Acad Radiol 22:33–49

2. Keenan KE, Biller JR, Delfino JG, Boss MA, Does MD, Evelhoch JL, Griswold MA, Gunter JL, Hinks RS, Hoffman SW, Kim G, Lattanzi R, Li X, Marinelli L, Metzger GJ, Mukherjee P, Nordstrom RJ, Peskin AP, Perez E, Russek SE, Sahiner B, Serkova N, Shukla-Dave A, Steckner M, Stupic KF, Wilmes LJ, Wu HH, Zhang H, Jackson EF, Sullivan DC (2019) Recommendations towards standards for quantitative MRI (qMRI) and outstanding needs. J Magn Reson Imaging 49:e26–e39

3. Tofts P (2003) Quantitative MRI of the brain: measuring changes caused by disease. Wiley, Chichester

4. Bojorquez JZ, Bricq S, Acquitter C, Brunotte F, Walker PM, Lalande A (2017) What are normal relaxation times of tissues at 3 T? Magn Reson Imaging 35:69–80

5. Marques JP, Simonis FFJ, Webb AG (2019) Low-field MRI: an MR physics perspective. J Magn Reson Imaging 49:1528–1542

6. Halse ME, Coy A, Dykstra R, Eccles C, Hunter M, Ward R, Callaghan PT (2006) A practical and flexible implementation of 3D MRI in the Earth's magnetic field. J Magn Reson 182:75–83

7. Sarracanie M, LaPierre CD, Salameh N, Waddington DEJ, Witzel T, Rosen MS (2015) Low-Cost High-Performance MRI. Sci Rep 5:15177

8. Cooley CZ, Stockmann JP, Armstrong BD, Sarracanie M, Lev MH, Rosen MS, Wald LL (2015) Two-dimensional imaging in a lightweight portable MRI scanner without gradient coils. Magn Reson Med 73:872–883

9. Lother S, Schiff SJ, Neuberger T, Jakob PM, Fidler F (2016) Design of a mobile, homogeneous, and efficient electromagnet with a large field of view for neonatal low-field MRI. Magma N Y N 29:691–698

10. Broche LM, Ross PJ, Davies GR, MacLeod M-J, Lurie DJ (2019) A whole-body fast field-cycling scanner for clinical molecular imaging studies. Sci Rep 9:10402

11. McDaniel PC, Cooley CZ, Stockmann JP, Wald LL (2019) The MR cap: a single-sided MRI system designed for potential point-of-care limited field-of-view brain imaging. Magn Reson Med 82:1946–1960

12. He Y, He W, Tan L, Chen F, Meng F, Feng H, Xu Z (2020) Use of 2.1 MHz MRI scanner for brain imaging and its preliminary results in stroke. J Magn Reson 319:106829

13. Cooley CZ, McDaniel PC, Stockmann JP, Srinivas SA, Cauley SF, Śliwiak M, Sappo CR, Vaughn CF, Guerin B, Rosen MS, Lev MH, Wald LL (2021) A portable scanner for magnetic resonance imaging of the brain. Nat Biomed Eng 5:229–239

14. O'Reilly T, Teeuwisse WM, Gans D, Koolstra K, Webb AG (2021) In vivo 3D brain and extremity MRI at 50 mT using a permanent magnet Halbach array. Magn Reson Med 85:495–505

15. Liu Y, Leong ATL, Zhao Y, Xiao L, Mak HKF, Tsang ACO, Lau GKK, Leung GKK, Wu EX (2021) A low-cost and shielding-free ultra-low-field brain MRI scanner. Nat Commun 12:7238

16. Bottomley PA, Foster TH, Argersinger RE, Pfeifer LM (1984) A review of normal tissue hydrogen NMR relaxation times and relaxation mechanisms from 1–100 MHz: dependence on tissue type, NMR frequency, temperature, species, excision, and age. Med Phys 11:425–448

17. Bydder GM, Steiner RE, Young IR, Hall AS, Thomas DJ, Marshall J, Pallis CA, Legg NJ (1982) Clinical NMR imaging of the brain: 140 cases. AJR Am J Roentgenol 139:215–236

18. O'Reilly T, Webb AG (2021) In vivo T1 and T2 relaxation time maps of brain tissue, skeletal muscle, and lipid measured in healthy volunteers at 50 mT. Magn Reson Med. https://doi.org/10.1002/mrm.29009

19. Keenan KE, Gimbutas Z, Dienstfrey A, Stupic KF, Boss MA, Russek SE, Chenevert TL, Prasad PV, Guo J, Reddick WE, Cecil KM, Shukla-Dave A, Aramburu Nunez D, Shridhar Konar A, Liu MZ, Jambawalikar SR, Schwartz LH, Zheng J, Hu P, Jackson EF

(2021) Multi-site, multi-platform comparison of MRI T1 measurement using the system phantom. PLoS One 16:e0252966

20. Bernstein MA, King KF, Zhou XJ (2004) Basic pulse sequences—inversion recovery. Handb MRI pulse Seq, 1st edn. Elsevier, London, pp 579–647

21. Cárdenas-Blanco A, Tejos C, Irarrazaval P, Cameron I (2008) Noise in magnitude magnetic resonance images. Concepts Magn Reson Part A 32A:409–416

22. Gudbjartsson H, Patz S (1995) The rician distribution of noisy MRI data. Magn Reson Med 34:910–914

23. Karlsen OT, Verhagen R, Bovée WMMJ (1999) Parameter estimation from Rician-distributed data sets using a maximum likelihood estimator: application to t1 and perfusion measurements. Magn Reson Med 41:614–623